IOP Publishing Inverse Problems

Inverse Problems **33** (2017) 055002 (22pp) https://doi.org/10.1088/1361-6420/aa5fc0

Numerical reconstruction of unknown Robin inclusions inside a heat conductor by a non-iterative method

Gen Nakamura[1] **and Haibing Wang**[2,3]

[1] Department of Mathematics, Hokkaido University, Sapporo 060-0810, Japan
[2] Department of Mathematics, Southeast University, Nanjing 210096, People's Republic of China

E-mail: hbwang@seu.edu.cn

Received 10 October 2016, revised 26 January 2017
Accepted for publication 10 February 2017
Published 3 March 2017

Abstract

Consider the problem of reconstructing unknown Robin inclusions inside a heat conductor from boundary measurements. This problem arises from active thermography and is formulated as an inverse boundary value problem for the heat equation. In our previous works, we proposed a sampling-type method for reconstructing the boundary of the Robin inclusion and gave its rigorous mathematical justification. This method is non-iterative and based on the characterization of the solution to the so-called Neumann-to-Dirichlet map gap equation. In this paper, we give a further investigation of the reconstruction method from both the theoretical and numerical points of view. First, we clarify the solvability of the Neumann-to-Dirichlet map gap equation and establish a relation of its solution to the Green function associated with an initial-boundary value problem for the heat equation inside the Robin inclusion. This naturally provides a way of computing this Green function from the Neumann-to-Dirichlet map and explains what is the input for the linear sampling method. Assuming that the Neumann-to-Dirichlet map gap equation has a unique solution, we also show the convergence of our method for noisy measurements. Second, we give the numerical implementation of the reconstruction method for two-dimensional spatial domains. The measurements for our inverse problem are simulated by solving the forward problem via the boundary integral equation method. Numerical results are presented to illustrate the efficiency and stability of the proposed method. By using a finite sequence of transient input over a time interval, we propose a new sampling method over the time interval by single measurement which is most likely to be practical.

[3] Author to whom any correspondence should be addressed.

1361-6420/17/055002+22$33.00

Keywords: inverse boundary value problem, heat equation, reconstruction method, Robin inclusion

(Some figures may appear in colour only in the online journal)

1. Introduction

Any anomaly in a conductor affects the propagation of the heat flow inside the conductor and as a result it also affects the temperature distribution on its surface. In many practical situations, the anomalies such as cavities, inclusions and cracks inside the conductor are unknown and hard to be detected directly. Active thermography is a widely used non-destructive testing technique in industrial engineering [22, 36], aiming to extract the internal structure of a heat conductor such as the size, location and shape of anomalies. Single measurement of active thermography is to inject a heat flux by using a heater, a flush lamp or laser to the conductor and measure the corresponding temperature distribution on its surface by using an infrared light camera. This is a non-contact and very fast measurement which can be easily repeated many times.

Let $\Omega \subset \mathbb{R}^d$ $(d = 2, 3)$ be a heat conductor and D be a Robin inclusion with impedance compactly embedded in Ω. We assume that the boundaries $\partial\Omega$ and ∂D of Ω and D belong to class C^2 and that $\Omega \setminus \overline{D}$ is connected. Injecting a heat flux g on $\partial\Omega$ over some time interval $(0, T)$, the corresponding temperature distribution $u(x, t)$ in $(\Omega \setminus \overline{D}) \times (0, T)$ can be modeled by the following initial-boundary value problem:

$$\begin{cases} (\partial_t - \Delta)u = 0 & \text{in } (\Omega \setminus \overline{D}) \times (0, T), \\ \partial_\nu u - \lambda u = 0 & \text{on } \partial D \times (0, T), \\ \partial_\nu u = g & \text{on } \partial\Omega \times (0, T), \\ u = 0 & \text{at } t = 0, \end{cases} \tag{1.1}$$

where $0 < \lambda = \lambda(x) \in C^1(\partial D)$ is the real-valued reciprocal of impedance and ν on ∂D (or $\partial\Omega$) is the unit normal vector directed into the exterior of D (or Ω). We have shown in [35] that the initial-boundary value problem (1.1) is well-posed in a suitable Sobolev space. Due to the positivity of λ, we can easily show that the influence of the input decays exponentially fast in time, which means that the single measurement is very fast and can be repeated many times. Based on this, we define the Neumann-to-Dirichlet map Λ_D by $\Lambda_D : g \mapsto u|_{\partial\Omega \times (0, T)}$, which is the idealized measurement for active thermography. When D is a rigid inclusion ($\lambda = \infty$) or a cavity ($\lambda = 0$); see, e.g. [27] for the physical explanation, we can formulate the initial-boundary value problem and define the Neumann-to-Dirichlet map analogously. The inverse problem for active thermography is to reconstruct D from the measured data Λ_D. We note that λ is unknown in our inverse problem. Actually, it can also be uniquely determined from boundary measurements [24].

There are many theoretical results for the above inverse problem; see, for example, [3, 13–15, 24], where some uniqueness results and stability estimates are established. It should be mentioned that in [14, 15] the unknown inclusions can depend on time. However, compared with inverse problems for elliptic equations, numerical studies for inverse boundary value problems for parabolic equations are rather limited. In [7, 8], Newton-type iteration algorithms based on domain derivatives are introduced. In [19, 20], the inverse problem is formulated as a shape optimization problem and is solved by optimization methods. A meshless method of

fundamental solutions is proposed in [12], where $u|_{t=0}$ is nonzero and D can depend on t. This method is also applied to simultaneously reconstruct D and λ for the Laplace equation case; see [27]. As for non-iterative reconstruction methods, we refer to [10, 11, 23, 25, 26, 29, 39] and the references therein, where the dynamical probe method and the enclosure method are developed. In addition, a numerical scheme for reconstructing the unknown defect via Feynman–Kac type formula is proposed in [28]. The authors established a linear sampling-type method for the heat equation in [21, 34]. Recently, this method was extended to the homogeneous Robin boundary condition case [35], where the short time asymptotic behavior of the indicator function is also investigated. Roughly speaking, our sampling method is based on the characterization of the solution to the so-called Neumann-to-Dirichlet map gap equation

$$(\Lambda_{\mathrm{D}} - \Lambda_{\varnothing})g = G^0_{(y,\,s)}(x,\,t), \tag{1.2}$$

where $\Lambda_{\varnothing}$ is the Neumann-to-Dirichlet map when there is no D in Ω, and $G^0_{(y,\,s)}(x,\,t) := G^0(x,\,t;\,y,\,s)$ is the Green function for the heat operator $\partial_t - \Delta$ in $\Omega \times (0,\,T)$ with homogeneous Neumann boundary condition. In terms of this characterization, the norm of the solution to (1.2) serves as an indicator function and the boundary of D can be reconstructed approximately by sampling points via computing the values of the indicator function at those points. It should be remarked that our method still works for nonzero initial condition, with some suitable modifications.

In this paper, assuming that D is a Robin inclusion, we give a further investigation of the linear sampling method for the heat equation. In [35], based on the factorization of the operator $F := \Lambda_{\mathrm{D}} - \Lambda_{\varnothing}$, we proved that for any $\varepsilon > 0$ there is a function g^{ε} such that $\|Fg^{\varepsilon} - G^0_{(y,\,s)}(x,\,t)\| \leqslant \varepsilon$, and the blow-up property of g^{ε} is shown. However, we do not know whether the equation (1.2) has an exact solution and what is the solution. So, as the first achievement of this paper, we clarify the solvability of the equation $Fg = G^0_{(y,\,s)}(x,\,t)$ and specify what is its solution if it exists. For $y \in \Omega \setminus D$, this equation has no solution. For $y \in D$, it will be shown that this equation has a solution if and only if the initial-boundary value problem

$$\begin{cases} (\partial_t - \Delta)v = 0 \quad \text{in } D \times (0,\,T), \\ (\partial_\nu - \lambda)v = -(\partial_{\nu(x)} - \lambda)G^0_{(y,\,s)}(x,\,t) \quad \text{on } (\partial D) \times (0,\,T), \\ v = 0 \quad \text{at } t = 0 \end{cases} \tag{1.3}$$

is solvable with the solution v satisfying the heat equation in $\Omega \times (0,\,T)$. Furthermore, if g is the solution to (1.2), then we have $g = \partial_\nu v|_{(\partial\Omega)\times(0,\,T)}$ and it is proved that $v|_{D\times(0,\,T)}$ is the difference between the Green functions $G^D_{(y,\,s)}(x,\,t)$ and $G^0_{(y,\,s)}(x,\,t)$, where $G^D_{(y,\,s)}(x,\,t)$ is the Green function of the heat operator in $D \times (0,\,T)$ with homogeneous Robin boundary condition. Hence, the linear sampling method provides a way of computing the Green function $G^D_{(y,\,s)}(x,\,t)$ from the Neumann-to-Dirichlet map Λ_{D} by solving the equation (1.2). A convergence result of our method for noisy measurements is also proved. The linear sampling method ejects an input g at time s creating a transient effect $G^D_{(y,\,s)}(x,\,t) - G^0_{(y,\,s)}(x,\,t)$ in D which can be extended to $\Omega \setminus \overline{D}$. Mathematically this effect in D is related to the reflected solution of the fundamental solution which blows up as y tends to ∂D.

The second achievement of the paper is providing a numerical implementation of the linear sampling method for the heat equation in two-dimensional spatial domains. Although the sampling-type method has been extensively studied in the field of inverse scattering problems from the numerical point of view; see [1, 2, 4–6, 9, 16, 17, 30–33, 37, 38] and the references therein, very few numerical results for the heat equation case are reported [35]. In this paper,

we give a complete investigation on the numerical implementation of the linear sampling method in the heat equation case utilizing the freedom to choose the time s. At first, we simulate the measurement data Λ_D by solving the forward problem (1.1), and compute the Neumann-to-Dirichlet map $\Lambda_\varnothing$ and the Green function $G^0_{(y,\,s)}(x,\,t)$ by solving the problem (1.1) with $D = \varnothing$. By expressing the solution as a single-layer heat potential, the initial-boundary value problem is transformed into a system of boundary integral equations [7, 8]. A numerical scheme for solving the resulting integral equations is presented. Then, we solve the discretized Neumann-to-Dirichlet map gap equation using the Tikhonov regularization method. We provide numerical results for the following three cases: (i) fixing the transient input time s and measuring over $(0,\,T)$; (ii) fixing s and measuring over a short time interval; (iii) giving transient inputs over a finite time series in $(0,\,T)$ and measuring over a short time interval. The set up for the last case provides a sampling method by single measurement and can be achieved for instance if the inputs over a time series can be generated by an electronic function generator for flash lamps or laser. Our numerical results greatly illustrate the effectiveness and feasibility of the reconstruction method. It can be easily seen that the linear sampling method for the heat equation allows more noise in the measured data, compared with that for inverse scattering problems. Actually, the stability of numerical reconstructions with respect to the noise has already been observed in [19]. Our method also provides good numerical results even for the case that there are two reasonably separated Robin inclusions inside the conductor.

The rest of this paper is organized as follows. In section 2, we give a further investigation of the linear sampling method for the heat equation. Some new results and observations are presented. Then, in section 3, we introduce a numerical scheme for solving the forward problem and simulate the Neumann-to-Dirichlet map. Numerical examples are provided in section 4 to show the effectiveness of the reconstruction method. Finally, in section 5, we give some conclusions.

2. Reconstruction method

In this section, we revisit the linear sampling method for the heat equation studied in [35]. First, we clarify the solvability of the Neumann-to-Dirichlet map gap equation. Second, if this equation is solvable, we further establish the relation of its solution to the Green function associated with an initial-boundary value problem for the heat equation in $D \times (0,\,T)$, and then give a way of computing this Green function from the Neumann-to-Dirichlet map. Third, we show a convergence result of our method for noisy measurements.

To begin with, we denote $X \times (0,\,T)$ and $\partial X \times (0,\,T)$ by X_T and $(\partial X)_T$, respectively, where X is a bounded domain in $\mathbb{R}^d$ and ∂X denotes its boundary. We now define the anisotropic Sobolev spaces which will be used in this paper. For $p,\,q \geqslant 0$ we define

$$H^{p,q}(\mathbb{R}^d \times \mathbb{R}) := L^2(\mathbb{R};\, H^p(\mathbb{R}^d)) \cap H^q(\mathbb{R};\, L^2(\mathbb{R}^d)).$$

For $p,\,q \leqslant 0$ we define the space $H^{p,q}$ by duality $H^{p,q}(\mathbb{R}^d \times \mathbb{R}) := (H^{-p,-q}(\mathbb{R}^d \times \mathbb{R}))'$. By $H^{p,q}(X_T)$ we denote the space of restrictions of elements in $H^{p,q}(\mathbb{R}^d \times \mathbb{R})$ to X_T. The space $H^{p,q}((\partial X)_T)$ is defined analogously. We also introduce the function space

$$\tilde{H}^{1,\frac{1}{2}}(X_T) := \left\{ u \in H^{1,\frac{1}{2}}(X \times (-\infty,\, T)) \,\middle|\, u(x,\,t) = 0 \ \text{for } t < 0 \right\}.$$

In [35], we proved that for any $g \in H^{-\frac{1}{2},-\frac{1}{4}}((\partial\Omega)_T)$ there exists a unique solution to (1.1) in $\tilde{H}^{1,\frac{1}{2}}((\Omega \setminus \overline{D})_T)$. Thus we define the Neumann-to-Dirichlet map by

$$\Lambda_{\mathrm{D}} : H^{-\frac{1}{2},-\frac{1}{4}}((\partial\Omega)_T) \to H^{\frac{1}{2},\frac{1}{4}}((\partial\Omega)_T), \quad g \mapsto u|_{(\partial\Omega)_T},$$

which is an idealized measurement data for active thermography. Our inverse problem is to reconstruct D from Λ_{D}.

We denote by $\Lambda_\varnothing$ the Neumann-to-Dirichlet map when there is no D inside Ω. That is, $\Lambda_\varnothing g := v|_{(\partial\Omega)_T}$ with v satisfying

$$\begin{cases} (\partial_t - \Delta)v = 0 & \text{in } \Omega_T, \\ \partial_\nu v = g & \text{on } (\partial\Omega)_T, \\ v = 0 & \text{at } t = 0. \end{cases} \tag{2.1}$$

Define the operator

$$F := \Lambda_{\mathrm{D}} - \Lambda_\varnothing.$$

Then our reconstruction scheme is based on the characterization of the solution to the Neumann-to-Dirichlet map gap equation

$$(Fg)(x, t) = G^0_{(y,s)}(x, t), \quad (x, t) \in (\partial\Omega)_T \tag{2.2}$$

for a fixed time $s \in (0, T)$ and the sampling point $y \in \Omega$.

At first, we address the solvability issue of the equation (2.2).

Theorem 2.1. *For $y \in D$ and any fixed $s \in (0, T)$, the Neumann-to-Dirichlet map gap equation (2.2) has a solution if and only if the initial-boundary value problem*

$$\begin{cases} (\partial_t - \Delta)v = 0 & \text{in } D_T, \\ (\partial_\nu - \lambda)v = -(\partial_\nu - \lambda)G^0_{(y,s)}(x, t) & \text{on } (\partial D)_T, \\ v = 0 & \text{at } t = 0 \end{cases} \tag{2.3}$$

is solvable with the solution v satisfying the heat equation in Ω_T with zero initial condition.

Proof. Assume that $g \in H^{-\frac{1}{2},-\frac{1}{4}}((\partial\Omega)_T)$ is the solution to (2.2). Let u and v be the solutions to (1.1) and (2.1), respectively. Then we have

$$\begin{cases} (\partial_t - \Delta)(u - v) = 0 & \text{in } (\Omega \setminus \overline{D})_T, \\ (\partial_\nu - \lambda)(u - v) = -(\partial_\nu - \lambda)v & \text{on } (\partial D)_T, \\ \partial_\nu(u - v) = 0 & \text{on } (\partial\Omega)_T, \\ u - v = 0 & \text{at } t = 0. \end{cases} \tag{2.4}$$

Note that

$$u - v = Fg = G^0_{(y,s)}(x, t) \quad \text{on } (\partial\Omega)_T$$

and

$$\partial_\nu(u - v) = 0 = \partial_\nu G^0_{(y,s)}(x, t) \quad \text{on } (\partial\Omega)_T.$$

By the unique continuation principle, we have

$$u - v = G^0_{(y,s)}(x, t) \quad \text{in } (\Omega \setminus \overline{D})_T. \tag{2.5}$$

Then it follows from (2.1) and (2.4) that

$$\begin{cases} (\partial_t - \Delta)v = 0 \quad \text{in } D_T, \\ (\partial_\nu - \lambda)v = -(\partial_\nu - \lambda)G^0_{(y,s)}(x,t) \quad \text{on } (\partial D)_T, \\ v = 0 \quad \text{at } t = 0. \end{cases} \tag{2.6}$$

On the other hand, if v is the solution to (2.3) satisfying the heat equation in Ω_T, then it can be shown that the function $g := \partial_\nu v|_{(\partial\Omega)_T}$ meets the equation (2.2). Indeed, we observe from (2.3) and (2.4) that

$$\begin{cases} (\partial_t - \Delta)(u - v - G^0_{(y,s)}) = 0 \quad \text{in } (\Omega \setminus \overline{D})_T, \\ (\partial_\nu - \lambda)(u - v - G^0_{(y,s)}) = 0 \quad \text{on } (\partial D)_T, \\ \partial_\nu(u - v - G^0_{(y,s)}) = 0 \quad \text{on } (\partial\Omega)_T, \\ u - v - G^0_{(y,s)} = 0 \quad \text{at } t = 0. \end{cases} \tag{2.7}$$

By the uniqueness of solutions to (2.7), we have

$$u - v = G^0_{(y,s)} \quad \text{in } (\Omega \setminus \overline{D})_T,$$

and hence

$$Fg = (u - v)|_{(\partial\Omega)_T} = G^0_{(y,s)}|_{(\partial\Omega)_T}.$$

The proof is complete. □

This theorem clarifies the solvability of the Neumann-to-Dirichlet map gap equation (2.2). Moreover, if g is the solution to (2.2), we let v be the solution to (2.1) with the boundary data $\partial_\nu v|_{(\partial\Omega)_T} = g$. Then we can conclude that

$$v = G^D_{(y,s)}(x,t) - G^0_{(y,s)}(x,t) \quad \text{in } D_T. \tag{2.8}$$

This result specifies what is the solution of the Neumann-to-Dirichlet map gap equation if it exists. We now give the proof of (2.8) as follows. Let $G_{(y,s)}(x,t) := G(x,t;y,s)$ be the fundamental solution to the heat equation in $\mathbb{R}^d$. Set

$$\hat{G}_{(y,s)}(x,t) := G^0_{(y,s)}(x,t) - G_{(y,s)}(x,t) \quad \text{in } \Omega_T, \tag{2.9}$$

which is the reflected solution of the fundamental solution in Ω_T and satisfies

$$\begin{cases} (\partial_t - \Delta)\hat{G}_{(y,s)}(x,t) = 0 \quad \text{in } \Omega_T, \\ \partial_\nu \hat{G}_{(y,s)}(x,t) = -\partial_\nu G_{(y,s)}(x,t) \quad \text{on } (\partial\Omega)_T, \\ \hat{G}_{(y,s)}(x,t) = 0 \quad \text{at } t = 0. \end{cases} \tag{2.10}$$

Here we would like to mention that the reflected solution $\hat{G}_{(y,s)}(x,t)$ and the Green function $G^0_{(y,s)}(x,t)$ are completely determined by the domain Ω, so they are known in our inverse problem. Set

$$\tilde{G}_{(y,s)}(x,t) := G^D_{(y,s)}(x,t) - G_{(y,s)}(x,t) \quad \text{in } D_T, \tag{2.11}$$

which is the reflected solution of the fundamental solution in D_T. Observe that $\tilde{G}_{(y,s)}(x,t)$ satisfies

$$\begin{cases} (\partial_t - \Delta)\tilde{G}_{(y,s)}(x,t) = 0 \quad \text{in } D_T, \\ (\partial_\nu - \lambda)\tilde{G}_{(y,s)}(x,t) = -(\partial_\nu - \lambda)G_{(y,s)}(x,t) \quad \text{on } (\partial D)_T, \\ \tilde{G}_{(y,s)}(x,t) = 0 \quad \text{at } t = 0. \end{cases} \tag{2.12}$$

Then we have

$$\begin{cases} (\partial_t - \Delta)(\tilde{G}_{(y,s)}(x,t) - \hat{G}_{(y,s)}(x,t) - v) = 0 \quad \text{in } D_T, \\ (\partial_\nu - \lambda)(\tilde{G}_{(y,s)}(x,t) - \hat{G}_{(y,s)}(x,t) - v) = 0 \quad \text{on } (\partial D)_T, \\ (\tilde{G}_{(y,s)}(x,t) - \hat{G}_{(y,s)}(x,t) - v) = 0 \quad \text{at } t = 0. \end{cases}$$

It implies that

$$v = \tilde{G}_{(y,s)}(x,t) - \hat{G}_{(y,s)}(x,t) \quad \text{in } D_T, \tag{2.13}$$

which yields (2.8). Thus, once we have the solution g to (2.2), we solve the initial-boundary value problem (2.1) with the boundary data $\partial_\nu v = g$ on $(\partial\Omega)_T$ and then compute the Green function $G^D_{(y,s)}(x,t) = v + G^0_{(y,s)}(x,t)$. In this sense, the linear sampling method for the heat equation actually provides a way of computing the Green function $G^D_{(y,s)}(x,t)$ from the Neumann-to-Dirichlet map Λ_D.

Theorem 2.2. *For $y \in \Omega \setminus D$ and any fixed $s \in (0,T)$, the Neumann-to-Dirichlet map gap equation (2.2) has no solution.*

Proof. Suppose that there exists a function $g \in H^{-\frac{1}{2},-\frac{1}{4}}((\partial D)_T)$ satisfying the equation (2.2). As shown in the proof of theorem 2.1, it follows from the unique continuation principle that

$$G^0_{(y,s)} = u - v \quad \text{in } (\Omega \setminus (\overline{D} \cup \{y\}))_T.$$

This implies that

$$\begin{aligned} \|G^0_{(y,s)}\|_{\tilde{H}^{1,\frac{1}{2}}((\Omega\setminus\overline{D})_T)} &= \|u - v\|_{\tilde{H}^{1,\frac{1}{2}}((\Omega\setminus\overline{D})_T)} \\ &\leqslant C\|(\partial_\nu - \lambda)v\|_{H^{-\frac{1}{2},-\frac{1}{4}}((\partial D)_T)} \\ &\leqslant \tilde{C}\|g\|_{H^{-\frac{1}{2},-\frac{1}{4}}((\partial\Omega)_T)} < \infty. \end{aligned}$$

However, for $y \in \Omega \setminus D$ we have $\|G^0_{(y,s)}\|_{\tilde{H}^{1,\frac{1}{2}}((\Omega\setminus\overline{D})_T)} = \infty$, which leads to a contradiction. This completes the proof. □

According to theorems 2.1 and 2.2, the solvability of (2.2) cannot be guaranteed. However, we can always find an approximate solution g in the sense that

$$\|Fg - G^0_{(y,s)}\|_{H^{\frac{1}{2},\frac{1}{4}}((\partial\Omega)_T)} < \varepsilon \tag{2.14}$$

for any $\varepsilon > 0$, due to the following properties of F concluded from our previous works in [35].

Theorem 2.3. *The operator F is injective, compact and has a dense range.*

We are now in a position to state the blow-up properties of the approximate solution g satisfying (2.14); see [35] for the proofs.

Theorem 2.4. *Let $s \in (0, T)$ be fixed. We have the following conclusions:*

(1) *if $y \in D$, then for any $\varepsilon > 0$ there exists a function $g \in H^{-\frac{1}{2},-\frac{1}{4}}((\partial\Omega)_T)$ satisfying*

$$\|Fg - G^0_{(y,s)}\|_{H^{\frac{1}{2},\frac{1}{4}}((\partial\Omega)_T)} < \varepsilon$$

such that

$$\lim_{y\to\partial D} \|g\|_{H^{-\frac{1}{2},-\frac{1}{4}}((\partial\Omega)_T)} = \infty \tag{2.15}$$

and

$$\lim_{y\to\partial D} \|Sg\|_{\tilde{H}^{1,\frac{1}{2}}(D_T)} = \infty, \tag{2.16}$$

where the operator S is defined by

$$S:\ H^{-\frac{1}{2},-\frac{1}{4}}((\partial\Omega)_T) \to \tilde{H}^{1,\frac{1}{2}}(D_T), \quad g \mapsto v|_{D_T},$$

with v being the solution to (2.1);

(2) *if $y \in \Omega \setminus D$, then for any ε, $\eta > 0$ there exists a function $g \in H^{-\frac{1}{2},-\frac{1}{4}}((\partial\Omega)_T)$ satisfying*

$$\|Fg - G^0_{(y,s)}\|_{H^{\frac{1}{2},\frac{1}{4}}((\partial\Omega)_T)} < \varepsilon + \eta$$

such that

$$\lim_{\eta\to 0} \|g\|_{H^{-\frac{1}{2},-\frac{1}{4}}((\partial\Omega)_T)} = \infty \tag{2.17}$$

and

$$\lim_{\eta\to 0} \|Sg\|_{\tilde{H}^{1,\frac{1}{2}}(D_T)} = \infty. \tag{2.18}$$

Based on theorem 2.4, we can define an indicator function

$$I(y) := \|g^y\|_{H^{-\frac{1}{2},-\frac{1}{4}}((\partial\Omega)_T)}$$

and reconstruct the location and shape of D by the following algorithm.

Algorithm 2.5.

1. Fix $s \in (0, T)$ and select a set of 'sampling points y' in Ω;
2. Compute an approximate solution to the equation (2.2);
3. Assert that $y \in D$ if and only if $I(y) \leqslant C$, where the cut-off constant C should be chosen properly.

In practice, the measured data always contain some noise, so the operator F cannot be given exactly and some regularization technique is needed in numerical implementations. Denote by F^δ the perturbed operator of F with

$$\|F^\delta - F\| \leqslant \delta,$$

where δ is the noise level and $\|\cdot\|$ is the operator norm. Using the Tikhonov regularization method, we construct an approximate solution to the perturbed Neumann-to-Dirichlet map gap equation

$$F^\delta g = G^0_{(y,s)}$$

by

$$g^y_{\alpha,\delta} := [\alpha I + (F^\delta)^* F^\delta]^{-1} \ (F^\delta)^* \ [G^0_{(y,s)}], \tag{2.19}$$

where $\alpha := \alpha(\delta)$ is the regularization parameter. Define the operator H by

$$H: \ g \mapsto -(\partial_\nu - \lambda) v|_{(\partial D)_T},$$

where v is the solution to (2.1). Then we have the following convergence result.

Theorem 2.6. *Let $y \in D$ and the Neumann-to-Dirichlet map gap equation (2.2) have a unique solution. Suppose that $\alpha(\delta) \to 0$ and $\frac{\delta}{\alpha^{3/2}(\delta)} \to 0$ as $\delta \to 0$. Then it holds that*

$$\| H[g^y_{\alpha,\delta}] - (\partial_\nu - \lambda) G^0_{(y,s)}|_{(\partial D)_T} \|_{H^{-\frac{1}{2},-\frac{1}{4}}((\partial D)_T)} \to 0 \quad \text{as } \delta \to 0. \tag{2.20}$$

Proof. By direct calculations, we have

$$\begin{aligned} H[g^y_{\alpha,\delta}] - h = {} & H\{[\alpha I + (F^\delta)^* F^\delta]^{-1} - [\alpha I + F^* F]^{-1}\} \ (F^\delta)^* \ [G^0_{(y,s)}] \\ & + H[\alpha I + F^* F]^{-1} \ [(F^\delta)^* - F^*] \ [G^0_{(y,s)}] \\ & + H[\alpha I + F^* F]^{-1} \ F^* \ [G^0_{(y,s)}] - (\partial_\nu - \lambda) G^0_{(y,s)}|_{(\partial D)_T}. \end{aligned} \tag{2.21}$$

Using the estimate

$$\| [\alpha I + (F^\delta)^* F^\delta]^{-1} - [\alpha I + F^* F]^{-1} \| \leqslant \frac{2\delta}{\alpha^{3/2}},$$

we have

$$\begin{aligned} & H\{[\alpha I + (F^\delta)^* F^\delta]^{-1} - [\alpha I + F^* F]^{-1}\} \ (F^\delta)^* \ [G^0_{(y,s)}] \\ & \leqslant \|H\| \ \|(F^\delta)^*\| \ \|G^0_{(y,s)}\| \frac{2\delta}{\alpha^{3/2}}. \end{aligned} \tag{2.22}$$

Note that the estimate

$$\|(\alpha I + B)^{-1}\| \leqslant \frac{1}{\alpha}$$

holds for any self-adjoint and positive operator B in Hilbert space. Then we obtain that

$$\| H[\alpha I + (F^\delta)^* F^\delta]^{-1} \ [(F^\delta)^* - F^*] \ [G^0_{(y,s)}] \| \leqslant \|H\| \ \|G^0_{(y,s)}\| \frac{\delta}{\alpha}. \tag{2.23}$$

Let g^y be the exact solution to (2.2) and define

$$g^y_\alpha := [\alpha I + F^* F]^{-1} \ F^* \ [G^0_{(y,s)}].$$

Then it follows that

$$g_\alpha^y \to g^y \quad \text{as } \alpha \to 0. \tag{2.24}$$

Let v_α be such that

$$\begin{cases} (\partial_t - \Delta) v_\alpha = 0 \quad \text{in } \Omega_T, \\ \partial_\nu v_\alpha = g_\alpha^y \quad \text{on } (\partial\Omega)_T, \\ v_\alpha = 0 \quad \text{at } t = 0. \end{cases}$$

Define v as the solution to

$$\begin{cases} (\partial_t - \Delta) v = 0 \quad \text{in } \Omega_T, \\ \partial_\nu v = g^y \quad \text{on } (\partial\Omega)_T, \\ v = 0 \quad \text{at } t = 0. \end{cases}$$

By the well-posedness of the above initial-boundary value problems, we obtain from (2.24) that $v_\alpha \to v$ in $\tilde{H}^{1,\frac{1}{2}}(\Omega_T)$ as $\alpha \to 0$, and hence $(\partial_\nu - \lambda) v_\alpha \to (\partial_\nu - \lambda) v$ in $H^{-\frac{1}{2},-\frac{1}{4}}((\partial D)_T)$ as $\alpha \to 0$. On the other hand, we note from the proof of theorem 2.1 that $(\partial_\nu - \lambda) v = -(\partial_\nu - \lambda) G^0_{(y,s)}$ on $(\partial D)_T$. Hence, we have

$$\| H[\alpha I + F^*F]^{-1} F^* [G^0_{(y,s)}] - (\partial_\nu - \lambda) G^0_{(y,s)}|_{(\partial D)_T} \|_{H^{-\frac{1}{2},-\frac{1}{4}}((\partial D)_T)} \to 0 \quad \text{as } \alpha \to 0.$$

Thus, the proof is completed by combining it with the estimates (2.22) and (2.23). □

Let $\bar{G}_{(y,s)}(x, t)$ be the solution to the following initial-boundary value problem:

$$\begin{cases} (\partial_t - \Delta) \bar{G}_{(y,s)}(x, t) = 0 \quad \text{in } D_T, \\ (\partial_\nu - \lambda) \bar{G}_{(y,s)}(x, t) = -(\partial_\nu - \lambda) G^0_{(y,s)}(x, t) \quad \text{on } (\partial D)_T, \\ \bar{G}_{(y,s)}(x, t) = 0 \quad \text{at } t = 0. \end{cases} \tag{2.25}$$

Take u and v as solutions to (1.1) and (2.1), respectively, where the Neumann boundary data on $(\partial\Omega)_T$ is given by (2.19). Then we obtain from (2.20) that

$$\| (\partial_\nu - \lambda)(v - \bar{G}_{(y,s)}) \|_{H^{-\frac{1}{2},-\frac{1}{4}}((\partial D)_T)} \to 0 \quad \text{as } \delta \to 0.$$

By the well-posedness of the initial-boundary value problem for the heat equation in D_T, we conclude that

$$\| S g^y_{\alpha,\delta} - \bar{G}_{(y,s)} \|_{\tilde{H}^{1,\frac{1}{2}}(D_T)} \to 0 \quad \text{as } \delta \to 0. \tag{2.26}$$

Note that

$$\bar{G}_{(y,s)}(x, t) = \tilde{G}_{(y,s)}(x, t) - \hat{G}_{(y,s)}(x, t) = G^D_{(y,s)}(x, t) - G^0_{(y,s)}(x, t) \quad \text{in } D_T.$$

Then we have

$$\| [S g^y_{\alpha,\delta} + G^0_{(y,s)}(x, t)] - G^D_{(y,s)}(x, t) \|_{\tilde{H}^{1,\frac{1}{2}}(D_T)} \to 0 \quad \text{as } \delta \to 0.$$

This gives the convergence of our algorithm for computing the Green function $G^D_{(y,s)}(x, t)$ from the Neumann-to-Dirichlet map.

3. Numerical realization of the Neumann-to-Dirichlet map

In this section, we present a numerical scheme to solve the forward problem (1.1) and simulate the operator $F = \Lambda_D - \Lambda_\varnothing$ for two-dimensional spatial domains. By expressing the solution as a single-layer heat potential, the initial-boundary value problem (1.1) is transformed into a system of boundary integral equations for an unknown density. To solve this system numerically, we apply a collocation method using piecewise constant interpolation with respect to the time variable on the equidistant grid $t_n := nT/N$, $n = 0, \cdots, N$, and then employ the Nyström method using the trapezoidal rule with respect to the space variable on the equidistant grid $\alpha_j := j\pi/M$, $j = 0, \cdots, 2M-1$; see [7, 8] for the details. In this way, the Neumann-to-Dirichlet map Λ_D is discretized as a matrix. In addition, the Green function $G^0_{(y,s)}(x, t)$ and the Neumann-to-Dirichlet map $\Lambda_\varnothing$ for the homogeneous conductor involved in (2.2) are also simulated by solving (2.1).

Define the following heat layer potentials:

$$V_{ij}[\varphi](x, t) := \int_0^t \int_{S_i} G(x, t; y, s)\varphi(y, s)\, d\sigma(y)ds, \quad (x, t) \in S_j \times (0, T),$$

$$N_{ij}[\varphi](x, t) := \int_0^t \int_{S_i} \frac{\partial G(x, t; y, s)}{\partial \nu(x)} \varphi(y, s)\, d\sigma(y)ds, \quad (x, t) \in S_j \times (0, T).$$

In this paper we take $i, j = 1, 2$ with $S_1 = \partial D$ and $S_2 = \partial\Omega$. First, we express the solution to (1.1) by the single-layer potential

$$\begin{aligned} u(x, t) = &\int_0^t \int_{\partial D} G(x, t; y, s)\varphi_1(y, s)\, d\sigma(y)ds \\ &+ \int_0^t \int_{\partial\Omega} G(x, t; y, s)\varphi_2(y, s)\, d\sigma(y)ds, \qquad (x, t) \in (\Omega \setminus \overline{D})_T, \end{aligned} \tag{3.1}$$

where φ_1 and φ_2 are density functions to be determined. Using jump relations of heat layer potentials, we can verify that $u(x, t)$ expressed by (3.1) is the solution to (1.1) provide that φ_1 and φ_2 satisfy

$$-\varphi_1 + 2N_{11}[\varphi_1] - 2\lambda V_{11}[\varphi_1] + 2N_{21}[\varphi_2] - 2\lambda V_{21}[\varphi_2] = 0, \tag{3.2}$$

$$2N_{12}[\varphi_1] + \varphi_2 + 2N_{22}[\varphi_2] = 2g. \tag{3.3}$$

Note that the integral kernels of N_{21}, V_{21} and N_{12} are smooth, while those of N_{11}, V_{11} and N_{22} are singular at $(x, t) = (y, s)$. To numerically solve the equations (3.2) and (3.3), we present a discretization scheme as follows.

Assume that the boundaries ∂D and $\partial\Omega$ have the parametric representations

$$\begin{aligned} \partial D &= \{x_1(\alpha) : x_1(\alpha) = (x_{11}(\alpha), x_{12}(\alpha)),\ 0 \leqslant \alpha \leqslant 2\pi\}, \\ \partial\Omega &= \{x_2(\alpha) : x_2(\alpha) = (x_{21}(\alpha), x_{22}(\alpha)),\ 0 \leqslant \alpha \leqslant 2\pi\}, \end{aligned}$$

where $x_{ij}(x)$ $(i, j = 1, 2)$ are of class C^2 and 2π-periodic functions. Notice that

$$\frac{\partial G(x, t; y, s)}{\partial \nu(x)} = \frac{(y - x)\cdot \nu(x)}{8\pi(t - s)^2} \exp\left(-\frac{|x - y|^2}{4(t - s)}\right), \quad t > s.$$

The unit outward normal vector on ∂D and $\partial\Omega$ are given by

$$\nu_1(\alpha) = \frac{(x_{12}'(\alpha),\ -x_{11}'(\alpha))}{|x_1'(\alpha)|} \quad \text{and} \quad \nu_2(\alpha) = \frac{(x_{22}'(\alpha),\ -x_{21}'(\alpha))}{|x_2'(\alpha)|},$$

respectively. Set $\tilde{\varphi}_i(\beta,\ s) := \varphi_i(x_i(\beta),\ s)$ for $i = 1,\ 2$, $r_{ij}(\alpha,\ \beta) = |x_j(\alpha) - x_i(\beta)|$, and

$$K_{ij}(\alpha,\ t;\ \beta,\ s) := G(x_j(\alpha),\ t;\ x_i(\beta),\ s),$$

$$L_{ij}(\alpha,\ t;\ \beta,\ s) := \frac{(x_i(\beta) - x_j(\alpha)) \cdot \nu_j(\alpha)|x_i'(\beta)|}{8\pi(t-s)^2} \exp\left(-\frac{r_{ij}^2(\alpha,\ \beta)}{4(t-s)}\right).$$

Then, by direct calculations, we have

$$\int_{t_{n-1}}^{t_n} K_{ij}(\alpha,\ t_n;\ \beta,\ s)\,\mathrm{d}s = \int_0^1 \frac{1}{4\pi t} \exp\left(-\frac{r_{ij}^2(\alpha,\ \beta)}{4t(t_n - t_{n-1})}\right)\mathrm{d}t,$$

$$\int_{t_{n-1}}^{t_n} L_{ij}(\alpha,\ t_n;\ \beta,\ s)\,\mathrm{d}s = \frac{(x_i(\beta) - x_j(\alpha)) \cdot \nu_j(\alpha)|x_i'(\beta)|}{2\pi r_{ij}^2(\alpha,\ \beta)} \exp\left(-\frac{r_{ij}^2(\alpha,\ \beta)}{4(t_n - t_{n-1})}\right).$$

For $m < n$, we have

$$\int_{t_{m-1}}^{t_m} K_{ij}(\alpha,\ t_n;\ \beta,\ s)\,\mathrm{d}s = \int_{t_n - t_m}^{t_n - t_{m-1}} \frac{1}{4\pi t} \exp\left(-\frac{r_{ij}^2(\alpha,\ \beta)}{4t}\right)\mathrm{d}t$$

$$= \int_0^{t_n - t_{m-1}} \frac{1}{4\pi t} \exp\left(-\frac{r_{ij}^2(\alpha,\ \beta)}{4t}\right)\mathrm{d}t - \int_0^{t_n - t_m} \frac{1}{4\pi t} \exp\left(-\frac{r_{ij}^2(\alpha,\ \beta)}{4t}\right)\mathrm{d}t$$

$$= \int_0^1 \frac{1}{4\pi t} \exp\left(-\frac{r_{ij}^2(\alpha,\ \beta)}{4t(t_n - t_{m-1})}\right)\mathrm{d}t - \int_0^1 \frac{1}{4\pi t} \exp\left(-\frac{r_{ij}^2(\alpha,\ \beta)}{4t(t_n - t_m)}\right)\mathrm{d}t$$

and

$$\int_{t_{m-1}}^{t_m} L_{ij}(\alpha,\ t_n;\ \beta,\ s)\,\mathrm{d}s = \frac{(x_i(\beta) - x_j(\alpha)) \cdot \nu_j(\alpha)|x_i'(\beta)|}{2\pi r_{ij}^2(\alpha,\ \beta)} \times \left\{\exp\left(-\frac{r_{ij}^2(\alpha,\ \beta)}{4(t_n - t_{m-1})}\right) - \exp\left(-\frac{r_{ij}^2(\alpha,\ \beta)}{4(t_n - t_m)}\right)\right\}.$$

Take

$$K_{ij}^{(p)}(\alpha,\ \beta) := \begin{cases} \dfrac{1}{4\pi} E_1\left(\dfrac{N r_{ij}^2(\alpha,\ \beta)}{4T}\right), & p = 0, \\ \dfrac{1}{4\pi} E_1\left(\dfrac{N r_{ij}^2(\alpha,\ \beta)}{4T(p+1)}\right) - \dfrac{1}{4\pi} E_1\left(\dfrac{N r_{ij}^2(\alpha,\ \beta)}{4Tp}\right), & p = 1,\ \cdots,\ N-1, \end{cases} \tag{3.4}$$

where E_1 is the exponential integral function defined by

$$E_1(z) = \int_1^{+\infty} \frac{\mathrm{e}^{-tz}}{t}\mathrm{d}t = \int_0^1 \frac{\mathrm{e}^{-z/u}}{u}\mathrm{d}u.$$

From the expansion

$$E_1(z) = -\gamma - \ln z - \sum_{n=1}^{+\infty} \frac{(-1)^n z^n}{n\,!\,n} \tag{3.5}$$

with $\gamma = 0.557\,21$ being Euler's constant, we conclude that $K_{jj}^{(0)}$ has a logarithmic singularity and can be decomposed into

$$K_{jj}^{(0)}(\alpha,\,\beta) = -\frac{1}{4\pi}\ln\left(\frac{4}{e}\sin^2\frac{\alpha-\beta}{2}\right) + \tilde{K}_{jj}^{(0)}(\alpha,\,\beta), \quad \alpha \neq \beta,$$

where

$$\tilde{K}_{jj}^{(0)}(\alpha,\,\beta) = K_{jj}^{(0)}(\alpha,\,\beta) + \frac{1}{4\pi}\ln\left(\frac{4}{e}\sin^2\frac{\alpha-\beta}{2}\right), \quad \alpha \neq \beta$$

with

$$\lim_{\beta\to\alpha} \tilde{K}_{jj}^{(0)}(\alpha,\,\beta) = -\frac{\gamma}{4\pi} - \frac{1}{4\pi}\ln\left(\frac{eN|x_j'(\alpha)|^2}{4T}\right).$$

In addition, it is evident that

$$\lim_{\beta\to\alpha} K_{jj}^{(p)}(\alpha,\,\beta) = \frac{1}{4\pi}\ln\frac{p+1}{p}, \quad p = 1,\,\cdots,\,N-1.$$

For $i \neq j$ the kernels $K_{ij}^{(p)}$ are continuous for $p = 0,\,1,\,\cdots,\,N-1$.

Set

$$L_{ij}^{(p)}(\alpha,\,\beta) := \begin{cases} \dfrac{(x_i(\beta)-x_j(\alpha))\cdot\nu_j(\alpha)|x_i'(\beta)|}{2\pi r_{ij}^2(\alpha,\,\beta)}\exp\left(-\dfrac{Nr_{ij}^2(\alpha,\,\beta)}{4T}\right), & p = 0, \\ \dfrac{(x_i(\beta)-x_j(\alpha))\cdot\nu_j(\alpha)|x_i'(\beta)|}{2\pi r_{ij}^2(\alpha,\,\beta)}\left\{\exp\left(-\dfrac{Nr_{ij}^2(\alpha,\,\beta)}{4T(p+1)}\right) - \exp\left(-\dfrac{Nr_{ij}^2(\alpha,\,\beta)}{4Tp}\right)\right\}, & p = 1,\,\cdots,\,N-1. \end{cases}$$

For $i = j$, we can easily show that

$$\lim_{\beta\to\alpha} L_{jj}^{(0)}(\alpha,\,\beta) = \frac{x_{j1}''(\alpha)x_{j2}'(\alpha) - x_{j1}'(\alpha)x_{j2}''(\alpha)}{4\pi|x_j'(\alpha)|^2}, \tag{3.6}$$

$$\lim_{\beta\to\alpha} L_{jj}^{(p)}(\alpha,\,\beta) = 0, \quad p = 1,\,\cdots,\,N-1. \tag{3.7}$$

For $i \neq j$, the kernels $L_{ij}^{(p)}$ are continuous for $p = 0,\,1,\,\cdots,\,N-1$.

Now we apply a collocation method using piecewise constant interpolation with respect to the time variable on the equidistant grid $t_n := nT/N$, $n = 0,\,1,\,\cdots,\,N$. That is, we approximate the density $\tilde{\varphi}_i(\beta,\,s)$ by

$$\tilde{\varphi}_i(\beta,\, s) \approx \sum_{n=1}^{N} \tilde{\varphi}_{i,n}(\beta)\Phi_n(s),$$

where $\tilde{\varphi}_{i,n}(\beta) := \tilde{\varphi}_i(\beta,\, t_n)$ and

$$\Phi_n(s) := \begin{cases} 1, & t_{n-1} < s \leqslant t_n, \\ 0, & \text{otherwise.} \end{cases}$$

Then, we have

$$\begin{aligned} V_{ij}[\varphi_i](x_j(\alpha),\, t_n) &= \int_0^{t_n}\int_0^{2\pi} K_{ij}(\alpha,\, t_n;\, \beta,\, s)\tilde{\varphi}_i(\beta,\, s)|x_i'(\beta)|\,\mathrm{d}\beta\mathrm{d}s \\ &= \int_0^{2\pi}\left(\sum_{m=1}^{n}\int_{t_{m-1}}^{t_m} K_{ij}(\alpha,\, t_n;\, \beta,\, s)\tilde{\varphi}_i(\beta,\, s)\mathrm{d}s\right)|x_i'(\beta)|\,\mathrm{d}\beta \\ &\approx \int_0^{2\pi}\left(\sum_{m=1}^{n}\tilde{\varphi}_{i,m}(\beta)\int_{t_{m-1}}^{t_m} K_{ij}(\alpha,\, t_n;\, \beta,\, s)\mathrm{d}s\right)|x_i'(\beta)|\,\mathrm{d}\beta \\ &\approx \sum_{m=1}^{n}\int_0^{2\pi} K_{ij}^{(n-m)}(\alpha,\, \beta)\tilde{\varphi}_{i,m}(\beta)|x_i'(\beta)|\,\mathrm{d}\beta \end{aligned}$$

and

$$\begin{aligned} N_{ij}[\varphi_i](x_j(\alpha),\, t_n) &= \int_0^{t_n}\int_0^{2\pi} L_{ij}(\alpha,\, t_n;\, \beta,\, s)\tilde{\varphi}_i(\beta,\, s)\,\mathrm{d}\beta\mathrm{d}s \\ &\approx \int_0^{2\pi}\left(\sum_{m=1}^{n}\tilde{\varphi}_{i,m}(\beta)\int_{t_{m-1}}^{t_m} L_{ij}(\alpha,\, t_n;\, \beta,\, s)\,\mathrm{d}s\right)\mathrm{d}\beta \\ &\approx \sum_{m=1}^{n}\int_0^{2\pi} L_{ij}^{(n-m)}(\alpha,\, \beta)\tilde{\varphi}_{i,m}(\beta)\,\mathrm{d}\beta. \end{aligned}$$

Using these approximations and setting $t = t_n$ for (3.2) and (3.3), we have the following Fredholm integral equations of the second kind:

$$\begin{aligned} &-\tilde{\varphi}_{1,n}(\alpha) + 2\sum_{k=1}^{2}\left(\int_0^{2\pi} L_{k1}^{(0)}(\alpha,\, \beta)\tilde{\varphi}_{k,n}(\beta)\,\mathrm{d}\beta - \tilde{\lambda}(\alpha)\int_0^{2\pi} K_{k1}^{(0)}(\alpha,\, \beta)|x_k'(\beta)|\tilde{\varphi}_{k,n}(\beta)\,\mathrm{d}\beta\right) \\ &= -2\sum_{k=1}^{2}\sum_{m=1}^{n-1}\left(\int_0^{2\pi} L_{k1}^{(n-m)}(\alpha,\, \beta)\tilde{\varphi}_{k,m}(\beta)\,\mathrm{d}\beta - \tilde{\lambda}(\alpha)\int_0^{2\pi} K_{k1}^{(n-m)}(\alpha,\, \beta)|x_k'(\beta)|\tilde{\varphi}_{k,m}(\beta)\,\mathrm{d}\beta\right), \end{aligned} \tag{3.8}$$

$$\begin{aligned} &\tilde{\varphi}_{2,n}(\alpha) + 2\sum_{k=1}^{2}\int_0^{2\pi} L_{k2}^{(0)}(\alpha,\, \beta)\tilde{\varphi}_{k,n}(\beta)\,\mathrm{d}\beta \\ &= \tilde{g}(\alpha,\, t_n) - 2\sum_{k=1}^{2}\sum_{m=1}^{n-1}\int_0^{2\pi} L_{k2}^{(n-m)}(\alpha,\, \beta)\tilde{\varphi}_{k,m}(\beta)\,\mathrm{d}\beta, \end{aligned} \tag{3.9}$$

where $\tilde{\lambda}(\alpha) = \lambda(x_1(\alpha))$ and $\tilde{g}(\alpha,\, t_n) = 2g(x_2(\alpha),\, t_n)$.

For the discretization with respect to the space variable, we apply the Nyström method to the above integral equations using the trapezoidal rule on the equidistant mesh $\beta_j := j\pi/M$, $j = 0,\, \cdots,\, 2M-1$. Especially, for the integral involving $K_{11}^{(0)}(\alpha,\, \beta)$, we need to treat the singular integral of the form

$$\int_0^{2\pi} \ln\left(\frac{4}{e}\sin^2\frac{\alpha-\beta}{2}\right)\varphi(\beta)\,\mathrm{d}\beta.$$

In fact, it can be computed approximately by the following quadrature rule

$$\int_0^{2\pi} \ln\left(\frac{4}{e}\sin^2\frac{\alpha_i-\beta}{2}\right)\varphi(\beta)\,\mathrm{d}\beta \approx 2\pi\sum_{j=0}^{2M-1} R_{|i-j|}\varphi(\alpha_j) \tag{3.10}$$

with the weights

$$R_j := -\frac{1}{2M}\left\{1+2\sum_{m=1}^{M-1}\frac{1}{m}\cos(m\alpha_j)+\frac{(-1)^j}{M}\right\},\quad j=0,\,1,\cdots,2M-1.$$

Thus we have the following linear system:

$$\begin{aligned}
&-\tilde{\varphi}_{1,n;i}+2\frac{\pi}{M}\sum_{k=1}^{2}\sum_{j=0}^{2M-1}L_{k1}^{(0)}(\beta_i,\,\beta_j)\tilde{\varphi}_{k,n;j}+\tilde{\lambda}(\beta_i)\sum_{j=0}^{2M-1}R_{|i-j|}|x_1'(\beta_j)|\tilde{\varphi}_{1,n;j}\\
&-2\tilde{\lambda}(\beta_i)\frac{\pi}{M}\sum_{j=0}^{2M-1}\tilde{K}_{11}^{(0)}(\beta_i,\,\beta_j)|x_1'(\beta_j)|\tilde{\varphi}_{1,n;j}-2\tilde{\lambda}(\beta_i)\frac{\pi}{M}\sum_{j=0}^{2M-1}K_{21}^{(0)}(\beta_i,\,\beta_j)|x_2'(\beta_j)|\tilde{\varphi}_{2,n;j}\\
&=-2\frac{\pi}{M}\sum_{k=1}^{2}\sum_{m=1}^{n-1}\sum_{j=0}^{2M-1}(L_{k1}^{(n-m)}(\beta_i,\,\beta_j)\tilde{\varphi}_{k,m;j}-\tilde{\lambda}(\beta_i)K_{k1}^{(n-m)}(\beta_i,\,\beta_j)|x_k'(\beta_j)|\tilde{\varphi}_{k,m;j}),
\end{aligned}\tag{3.11}$$

$$\begin{aligned}
&\tilde{\varphi}_{2,n;i}+2\frac{\pi}{M}\sum_{k=1}^{2}\sum_{j=0}^{2M-1}L_{k2}^{(0)}(\beta_i,\,\beta_j)\tilde{\varphi}_{k,n;j}\\
&=\tilde{g}(\beta_i,\,t_n)-2\frac{\pi}{M}\sum_{k=1}^{2}\sum_{m=1}^{n-1}\sum_{j=0}^{2M-1}L_{k2}^{(n-m)}(\beta_i,\,\beta_j)\tilde{\varphi}_{k,m;j},
\end{aligned}\tag{3.12}$$

for approximate values $\tilde{\varphi}_{1,n;i}\approx\tilde{\varphi}_{1,n}(\beta_i)$, $\tilde{\varphi}_{2,n;i}\approx\tilde{\varphi}_{2,n}(\beta_i)$, $i=0,\,\cdots,\,2M-1$, $n=1,\,\cdots,\,N$. This system can be solved recursively for $n=1,\,\cdots,\,N$.

Once we obtain the density functions φ_1 and φ_2 approximately by solving the above linear system, we can compute $u(x,\,t)|_{(\partial\Omega)_T}$ in terms of (3.1):

$$\begin{aligned}
u(x_2(\beta_i),\,t_n)\approx{}&\frac{\pi}{M}\sum_{m=1}^{n}\sum_{j=0}^{2M-1}K_{12}^{(n-m)}(\beta_i,\,\beta_j)|x_1'(\beta_j)|\tilde{\varphi}_{1,m;j}-\frac{1}{2}\sum_{j=0}^{2M-1}R_{|i-j|}|x_2'(\beta_j)|\tilde{\varphi}_{2,n;j}\\
&+\frac{\pi}{M}\sum_{j=0}^{2M-1}\tilde{K}_{22}^{(0)}(\beta_i,\,\beta_j)|x_2'(\beta_j)|\tilde{\varphi}_{2,n;j}\\
&+\frac{\pi}{M}\sum_{m=1}^{n-1}\sum_{j=0}^{2M-1}K_{22}^{(n-m)}(\beta_i,\,\beta_j)|x_2'(\beta_j)|\tilde{\varphi}_{2,m;j}
\end{aligned}\tag{3.13}$$

for $i=0,\,1,\,\cdots,\,2M-1,\ n=1,\,2,\,\cdots,\,N$.

Let

$$\mathbb{U}=(u(x_2(\beta_0),\,t_1),\,\cdots,\,u(x_2(\beta_{2M-1}),\,t_1),\,\cdots,\,u(x_2(\beta_0),\,t_N),\,\cdots,\,u(x_2(\beta_{2M-1}),\,t_N))^T,$$

$$\beta=(g(x_2(\beta_0),\,t_1),\,\cdots,\,g(x_2(\beta_{2M-1}),\,t_1),\,\cdots,\,g(x_2(\beta_0),\,t_N),\,\cdots,\,g(x_2(\beta_{2M-1}),\,t_N))^T.$$

Then, in view of (3.11)–(3.13) we can assemble a matrix $\mathbb{A}_{\mathrm{D}} \in \mathbb{R}^{2MN\times 2MN}$ such that

$$\mathbb{U} = \mathbb{A}_{\mathrm{D}}\,\beta. \tag{3.14}$$

Thus, we finally get the discretized version $\mathbb{A}_{\mathrm{D}}$ of the Neumann-to-Dirichlet map Λ_{D}, which is the measured data for our inverse problem.

In the same way as described above, we can obtain the discretized version $\mathbb{A}_{\varnothing}$ of the Neumann-to-Dirichlet map $\Lambda_{\varnothing}$ by considering the following initial-boundary value problem:

$$\begin{cases} (\partial_t - \Delta)v = 0 \quad \text{in } \Omega_T\,, \\ \partial_\nu v = g \quad \text{on } (\partial\Omega)_T, \\ v = 0 \quad \text{at } t = 0. \end{cases} \tag{3.15}$$

So the operator F is discretized as the matrix $\mathbb{F} := \mathbb{A}_{\mathrm{D}} - \mathbb{A}_{\varnothing}$. Note that the Green function $G^0_{(y,\,s)}(x,\,t) = G_{(y,\,s)}(x,\,t) + \hat{G}_{(y,\,s)}(x,\,t)$, where $\hat{G}_{(y,\,s)}(x,\,t)$ satisfies (3.15) with $g = -\partial_{\nu(x)}G_{(y,\,s)}(x,\,t)$. The function $\hat{G}_{(y,\,s)}(x,\,t)$ can be computed by the above numerical method and the Green function $G^0_{(y,\,s)}(x,\,t)$ are therefore synthesized. Let

$$\begin{aligned}\mathbb{G}_{(y,\,s)} = (&G^0_{(y,\,s)}(x_2(\beta_0),\,t_1),\,\cdots,\,G^0_{(y,\,s)}(x_2(\beta_{2M-1}),\,t_1),\\ &\cdots,\,G^0_{(y,\,s)}(x_2(\beta_0),\,t_N),\,\cdots,\,G^0_{(y,\,s)}(x_2(\beta_{2M-1}),\,t_N))^T.\end{aligned}$$

Then we are led to the following linear equation:

$$\mathbb{F}\,\beta = \mathbb{G}_{(y,\,s)}, \tag{3.16}$$

which is the discretized version of the Neumann-to-Dirichlet map gap equation (2.2).

4. Numerical results and discussions

In this section, we present some numerical results to show the performance of the linear sampling method for the heat equation. First, we simulate the operator $F = \Lambda_{\mathrm{D}} - \Lambda_{\varnothing}$ and compute the Green function $G^0_{(y,\,s)}(x,\,t)$ by the numerical scheme provided in section 3. Then, taking the synthetic data as our measurements, the discretized Neumann-to-Dirichlet map gap equation (3.16) is solved by the classical Tikhonov regularization method, where the regularization parameter is chosen by generalized cross validation criterion and the Matlab code developed in [18] is used in our computations. In the first example, we implement the reconstruction method for one Robin inclusion of three different shapes. The second example is devoted to the numerical reconstruction of two well-separated Robin inclusions inside the heat conductor. We also test the method with short time measurements in the last two examples.

In all examples, we take $N = 100$, $M = 16$. Based on the numerical scheme for solving the forward problem, we obtain a 3200×3200 matrix $\mathbb{F} := (f_{ij})$ which is the discretized version of the operator $F = \Lambda_{\mathrm{D}} - \Lambda_{\varnothing}$. The uniform random noise is added to $\mathbb{F}$ via

$$f^{\delta}_{ij} = f_{ij} \times (1 + \delta\, rd_{ij}),$$

where δ is the noise level and (rd_{ij}) is a matrix whose elements are normally distributed with mean value 0 and standard deviation 1. In numerics, we let Ω be a circle with radius r and center at the origin. We choose 20×32 sampling points in Ω specified by

$$y_{ij} = r_i(\cos(\alpha_j),\,\sin(\alpha_j)), \quad r_i = \frac{r}{20}i,\ \alpha_j = \frac{\pi}{16}j, \quad i = 1,\cdots,20,\ j = 1,\cdots,32. \tag{4.1}$$

For each sampling point y_{ij}, we solve the discretized Neumann-to-Dirichlet map gap equation (3.16) by the Tikhonov regularization method and compute the indicator function $I(y_{ij})$ defined by

$$I(y_{ij}) := 1/\ln(\|g^{y_{ij}}\|_{L^2}). \tag{4.2}$$

Example 1. We test the reconstruction method for one Robin inclusion. Let Ω be a circle with radius 3 centered at the origin. For D, we consider the following three different shapes, namely, kite-shaped, boat-shaped and pear-shaped domains parameterized by

'Kite' : $\partial D = \{(\cos(\alpha) + 0.65\cos(2\alpha) - 0.65, 1.5\sin(\alpha)) : \alpha \in [0, 2\pi]\}$;
'Boat' : $\partial D = \{(0.25\cos(\alpha) - 0.05\sin(4\alpha), -0.75\sin(\alpha)) : \alpha \in [0, 2\pi]\}$;
'Pear' : $\partial D = \{(2 + 0.3\cos(3\alpha))(\cos(\alpha), \sin(\alpha)) : \alpha \in [0, 2\pi]\}$.

Set $T = 1$, $\lambda = 1$, $\delta = 0.05$.

Theoretically, our reconstruction method should work for any $s \in (0, T)$, so we test it for each shape using $s = 0.3$ and $s = 0.6$. In figures 1–3, we show the numerical reconstructions of D with 100 contour lines of the indicator function. It can be easily seen that the L^2 norm of g^y becomes significantly large as the sampling point y approaches the boundary ∂D and remains large outside D. Moreover, changing the values of s does not have evident influence on the reconstruction results. These observations greatly support our theoretical analysis. The numerical results indicate that our reconstruction method is effective and works for Robin inclusions of different shapes. We also observe that the linear sampling method for the heat equation has a high tolerance for the measurement noise, compared with inverse scattering problems in frequency domain. This may be benefited from the dynamical measured data.

Example 2. We test the reconstruction method for the case when there are two well-separated Robin inclusions in the heat conductor. Let Ω be a circle with radius 6 centered at the origin, and D_1, D_2 have different shapes parameterized by

'Kite'and'Pear' : $\partial D_1 = \{(\cos(\alpha) + 0.65\cos(2\alpha) - 2.65, 1.5\sin(\alpha)) : \alpha \in [0, 2\pi]\}$,
$\partial D_2 = \{(2 + 0.3\cos(3\alpha))(\cos(\alpha) + 2, \sin(\alpha)) : \alpha \in [0, 2\pi]\}$;
'Boat'and'Pear' : $\partial D_1 = \{(0.25\cos(\alpha) - 0.05\sin(4\alpha) - 2, -0.75\sin(\alpha)) : \alpha \in [0, 2\pi]\}$,
$\partial D_2 = \{(2 + 0.3\cos(3\alpha))(\cos(\alpha) + 2, \sin(\alpha)) : \alpha \in [0, 2\pi]\}$.

Set $T = 1$ and the Robin coefficients on ∂D_1 and ∂D_2 are taken as $\lambda_1 = \lambda_2 = 1$.

In figures 4 and 5, we show the numerical reconstructions of two Robin inclusions using 100 contour lines, where s is taken to be 0.3. When these are reasonably well-separated, the location and shape of each of them can be approximately reconstructed, although the adjacent parts cannot be captured very well. But as the distance between them becomes large, the reconstruction results will be greatly improved.

Example 3. We test the reconstruction method for one Robin inclusion with short time measurements. Let Ω be a circle with radius 3 centered at the origin and D be the pear-shaped domain given in example 1. T and λ are set to be the same as in example 1.

Instead of the full measurements Λ_D for $t \in (0, T)$, we here use the short time measurements Λ_D with t in a small interval $(s_0, s_0 + s_1)$. The numerical reconstructions of D are shown in figure 6, where we fix $s_1 = 0.3$ and test the method for $s_0 = 0.3$ and $s_0 = 0.6$, respectively.

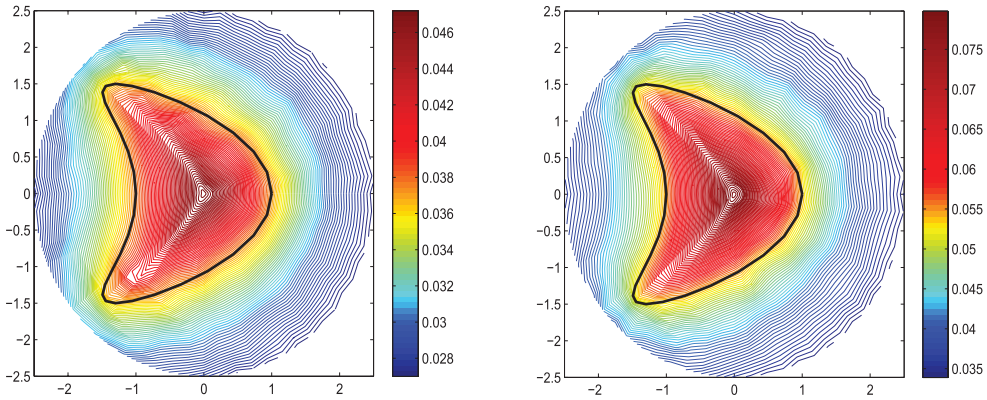

Figure 1. Kite-shaped domain: $s = 0.3$ (left), $s = 0.6$ (right).

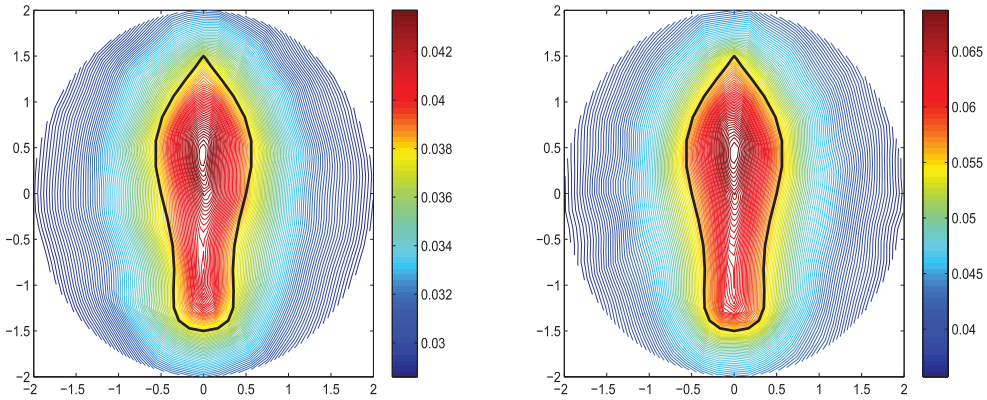

Figure 2. Boat-shaped domain: $s = 0.3$ (left), $s = 0.6$ (right).

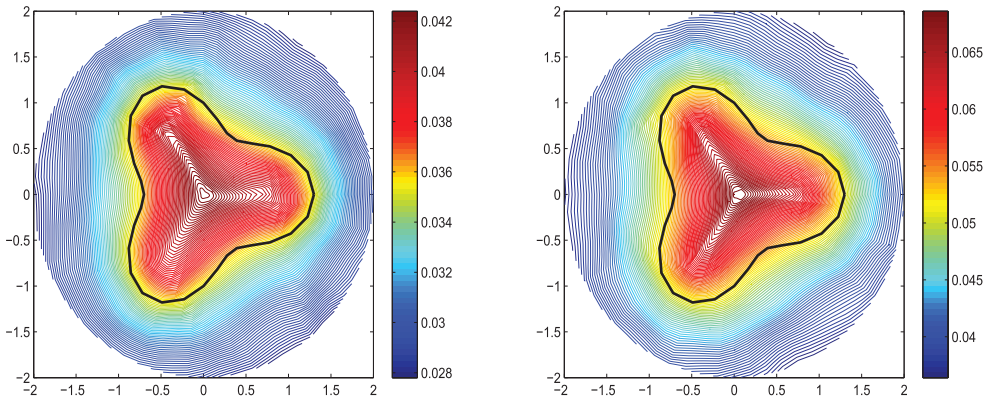

Figure 3. Pear-shaped domain: $s = 0.3$ (left), $s = 0.6$ (right).

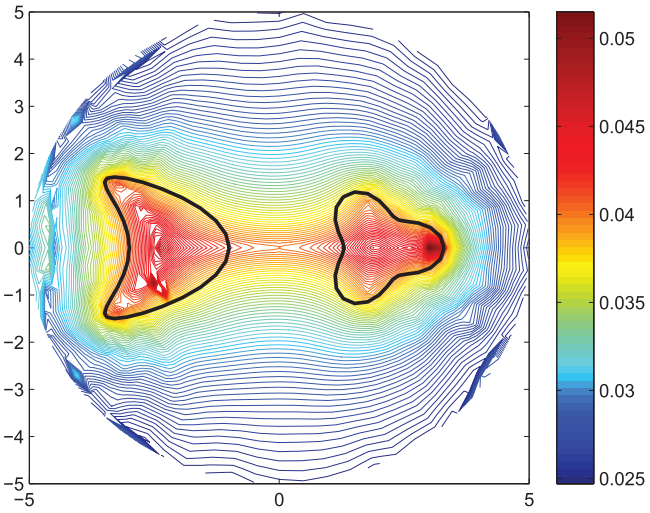

Figure 4. Kite-shaped and pear-shaped domains: $s = 0.3$.

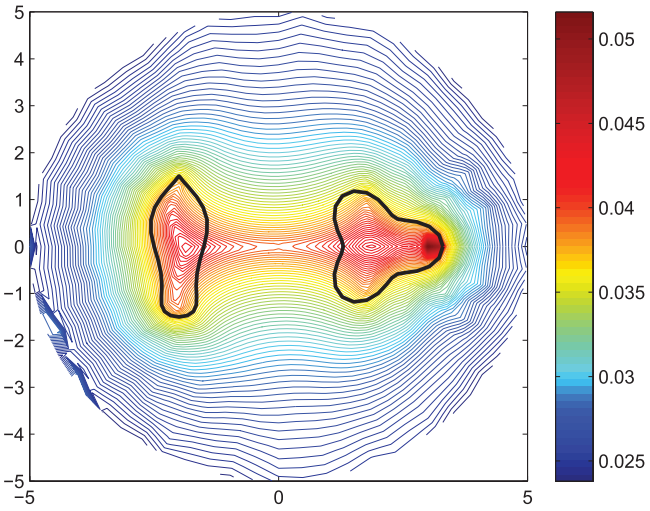

Figure 5. Boat-shaped and pear-shaped domains: $s = 0.3$.

The numerical results indicate that some information on D could still be captured, although the shape may not be clearly recovered.

Now we propose a new sampling method which can approximately recover ∂D by a single measurement over $(0,T)$. This kind of sampling method is most likely to be practical.

Example 4. Let the configuration of the conductor be the same as that in example 3. Let $\{y_{ij}\}$ be the sampling points given by (4.1). Consider the absolute linear order $\prec$ for any two different pairs (ℓ, m) and (ℓ', m') of $y_{\ell,m}$ and $y_{\ell',m'}$ by

$$(\ell, m) \prec (\ell', m') \text{ if either the case } \ell' > \ell \text{ or the case } \ell' = \ell \text{ and } m' > m.$$

Numerate these pairs (ℓ, m) of $y_{\ell,m}$'s by this linear absolute order so that $\{(\ell, m)\} = \{k\}$ with

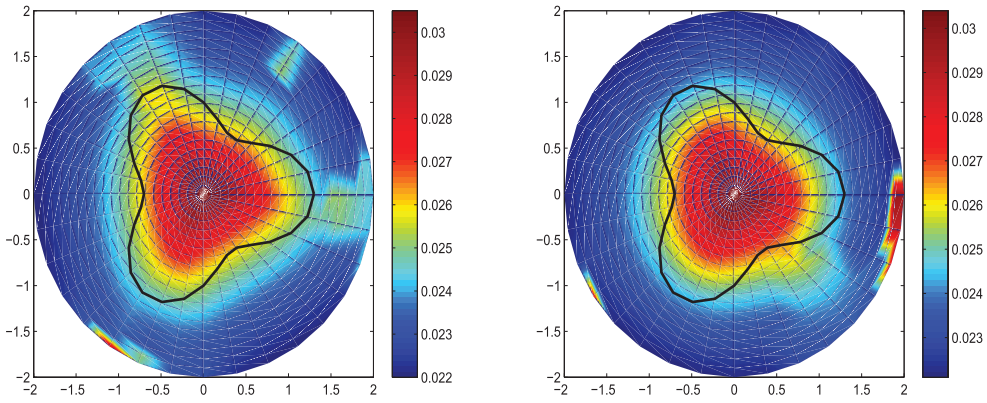

Figure 6. Pear-shaped domain with short time measurement: $s = 0.3$ (left), $s = 0.6$ (right).

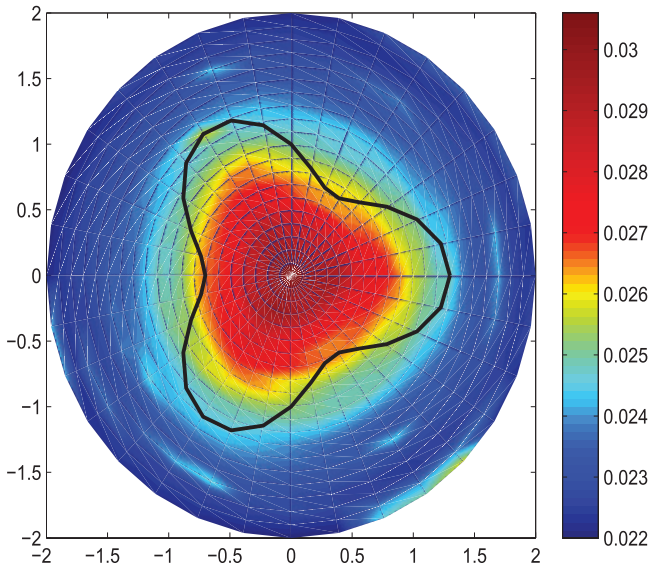

Figure 7. Pear-shaped domain with a time series.

$k = 1, 2, \cdots, 640$. Consider a finite time series $\{\tilde{s}_k\}_{k=1}^{640} \subset (0, T)$ such that $\tilde{s}_1 < \tilde{s}_2 < \cdots < \tilde{s}_{640}$. At each $\tilde{s}_k$ we give the transient input as before and measure over $(\tilde{s}_k, \tilde{s}_k + \tau)$ with τ being a small number. With these measurements, we get the numerical reconstruction of D as displayed in figure 7.

5. Conclusions

This paper gave a further investigation of the linear sampling method for the heat equation, based on our previous works in [21, 35]. We first clarified the solvability of the Neumann-to-Dirichlet map gap equation and established the relation of its solution to the Green function $G^D_{(y,s)}(x, t)$ in D_T. Consequently, we showed what is the input for the linear sampling method and provided a way of computing the Green function associated with an interior

initial-boundary value problem in D_T. Using the boundary integral equation method for the heat equation, we presented a numerical scheme for simulating the Neumann-to-Dirichlet map and the Green function $G^0_{(y,s)}(x, t)$ which is known for our inverse problem. The discretized Neumann-to-Dirichlet map gap equation was solved by using the Tikhonov regularization method. As for the numerical experiments, we showed that the linear sampling method for the heat equation is effective and relatively stable to noise. We also proposed a new sampling method which may approximately recover ∂D from single measurement over a time interval. In future, we intend to investigate our method for the case that D depends on time.

Acknowledgment

The authors would like to thank the referees for their careful reading and valuable suggestions, which made the paper much improved. This work is supported by National Natural Science Foundation of China (Nos. 11301075, 11671082). The first author is also supported by a Grant-in-Aid for Scientific Research (15K21766) of the Japan Society for the Promotion of Science. The second author is also supported by Natural Science Foundation of Jiangsu Province (No. BK20130594) and Qing Lan Project of Jiangsu Province.

References

[1] Arens T and Lechleiter A 2009 The linear sampling method revisited *J. Integral Equ. Appl.* **21** 179–202
[2] Audibert L and Haddar H 2014 A generalized formulation of the linear sampling method with exact characterization of targets in terms of far field measurements *Inverse Problems* **30** 035011
[3] Bacchelli V, Di Cristo M, Sincich E and Vessella S 2014 A parabolic inverse problem with mixed boundary data. Stability estimates for the unknown boundary and impedance *Trans. Am. Math. Soc.* **366** 3965–95
[4] Cakoni F and Colton D 2006 *Qualitative Methods in Inverse Scattering Theory* (Springer: Berlin)
[5] Cakoni F, Colton D and Monk P 2011 *The Linear Sampling Method in Inverse Electromagnetic Scattering* (Philadelphia: SIAM)
[6] Cakoni F, Di Cristo M and Sun J G 2012 A multistep reciprocity gap functional method for the inverse problem in a multilayered medium *Complex Var. Elliptic Equ.* **57** 261–76
[7] Chapko R, Kress R and Yoon J R 1998 On the numerical solution of an inverse boundary value problem for the heat equation *Inverse Problems* **14** 853–67
[8] Chapko R, Kress R and Yoon J R 1999 An inverse boundary value problem for the heat equation: the Neumann condition *Inverse Problems* **15** 1033–46
[9] Chen Q, Haddar H, Lechleiter A and Monk P 2010 A sampling method for inverse scattering in the time domain *Inverse Problems* **26** 085001
[10] Daido Y, Kang H and Nakamura G 2007 A probe method for the inverse boundary value problem of non-stationary heat equations *Inverse Problems* **23** 1787–800
[11] Daido Y, Lei Y, Liu J J and Nakamura G 2009 Numerical implementations of dynamical probe method for non-stationary heat equation *Appl. Math. Comput.* **211** 510–21
[12] Dawson M, Borman D, Hammond R B, Lesnic D and Rhodes D 2013 A meshless method for solving a two-dimensional transient inverse geometric problem *Int. J. Numer. Methods Heat Fluid Flow* **23** 790–817
[13] Di Cristo M, Rondi L and Vessella S 2006 Stability properties of an inverse parabolic problem with unknown boundaries *Ann. Mat. Pura Appl.* **185** 223–55
[14] Di Cristo M and Vessella S 2010 Stable determination of the discontinuous conductivity coefficient of a parabolic equation *SIAM J. Math. Anal.* **42** 183–217
[15] Elayyan A and Isakov V 1997 On uniqueness of recovery of the discontinuous conductivity coefficient of a parabolic equation *SIAM J. Math. Anal.* **28** 49–59
[16] Guo Y, Monk P and Colton D 2013 Toward a time domain approach to the linear sampling method *Inverse Problems* **29** 095016

[17] Haddar H, Lechleiter A and Marmorat S 2014 An improved time domain linear sampling method for Robin and Neumann obstacles *Appl. Anal.* **93** 369–90
[18] Hansen P C 1994 Regularization tools: a Matlab package for analysis and solution of discrete ill-posed problems *Numer. Algorithms* **6** 1–35
[19] Harbrecht H and Tausch J 2011 An efficient numerical method for a shape-identification problem arising from the heat equation *Inverse Problems* **27** 065013
[20] Harbrecht H and Tausch J 2013 On the numerical solution of a shape optimization problem for the heat equation *SIAM J. Sci. Comput.* **35** A104–21
[21] Heck H, Nakamura G and Wang H B 2012 Linear sampling method for identifying cavities in a heat conductor *Inverse Problems* **28** 075014
[22] Ibarra-Castanedo C, Piau J, Guilbert S, Avdelidis N P, Genest M, Bendada A and Maldague X P V 2009 Comparative study of active thermography techniques for the nondestructive evaluation of honeycomb structures *Res. Nondestruct. Eval.* **20** 1–31
[23] Ikehata M and Kawashita M 2009 The enclosure method for the heat equation *Inverse Problems* **25** 075005
[24] Isakov V 2008 On uniqueness of obstacles and boundary conditions from restricted dynamical and scattering data *Inverse Problems Imaging* **2** 151–65
[25] Isakov V, Kim K and Nakamura G 2010 Reconstruction of an unknown inclusion by thermography *Ann. Scuola Norm. Super. Pisa Cl. Sci.* **9** 725–58
[26] Isozaki H, Poisson O, Siltanen S and Tamminen J 2012 Probing for inclusions in heat conductive bodies *Inverse Problems Imaging* **6** 423–46
[27] Karageorghis A, Bin-Mohsin B, Lesnic D and Marin L 2015 Simultaneous numerical determination of a corroded boundary and its admittance *Inverse Problems Sci. Eng.* **23** 1120–37
[28] Kawakami H 2015 Reconstruction algorithm for unknown cavities via Feynman–Kac type formula *Comput. Opt. Appl.* **61** 101–33
[29] Kim K and Nakamura G 2011 Inverse boundary value problem for anisotropic heat operators *J. Phys.: Conf. Ser.* **290** 012007
[30] Kirsch A and Grinberg N 2008 *The Factorization Method for Inverse Problems* (Oxford: Oxford University Press)
[31] Li J Z, Liu H Y and Wang Q 2014 Enhanced multilevel linear sampling methods for inverse scattering problems *J. Comput. Phys.* **257** 554–71
[32] Li J Z, Liu H Y and Zou J 2009 Strengthened linear sampling method with a reference ball *SIAM J. Sci. Comput.* **31** 4013–40
[33] Li J Z, Liu H Y and Zou J 2008 Multilevel linear sampling method for inverse scattering problems *SIAM J. Sci. Comput.* **30** 1228–50
[34] Nakamura G and Wang H B 2013 Linear sampling method for the heat equation with inclusions *Inverse Problems* **29** 104015
[35] Nakamura G and Wang H B 2015 Reconstruction of an unknown cavity with Robin boundary condition inside a heat conductor *Inverse Problems* **31** 125001
[36] Patel P M, Lau S K and Almond D P 1992 A review of image analysis techniques applied in transient thermographic nondestructive testing *Nondestructive. Test. Eval.* **6** 343–64
[37] Thành N T and Sini M 2010 An analysis of the accuracy of the linear sampling method for an acoustic inverse obstacle scattering problem *Inverse Problems* **26** 015010
[38] Thành N T and Sini M 2010 Accuracy of the linear sampling method for inverse obstacle scattering: effect of geometrical and physical parameters *Inverse Problems* **26** 125004
[39] Yi L, Kim K and Nakamura G 2010 Numerical implementation for a 2D thermal inhomogeneity through the dynamical probe method *J. Comput. Math.* **28** 87–104